Journal of the European Ceramic Society **18** (1998) 1–13

PII: S0955-2219(97)00092-7
0955-2219/98/$19.00 + 0.00

Grain Shape in Sintered Submicrometre Alumina

Andreas Krell and Peter Obenaus

Fraunhofer Institut für Keramische Technologien und Sinterwerkstoffe (IKTS), D-01277 Dresden, Germany

(Received 27 November 1996; accepted 27 February 1997)

Abstract

The study compares different approaches to describe quantitatively crystallite shapes in alumina microstructures with grain sizes 0·2–2 μm. A method is reinvestigated that characterizes the 3-dimensional shape of equiaxed grains and distinguishes equiaxed and non-equiaxed characters by analysing plain sections without additionally required assumptions. Other parameters which describe the shape after anistropic grain growth are evaluated regarding their ability to identify non-equiaxed shapes with small aspect ratios. The analysis is applied to a wide spectrum of dense microstructures produced by powder and by sol–gel approaches. Whereas each of the procedures can give microstructures that come close to the parameter range associated with equiaxed shapes it is, in fact, impossible to produce alumina microstructures with predominantly equiaxed crystallites. © *1997 Elsevier Science Limited.*

1 Introduction—Grain Shape and Toughness in Submicrometre Alumina

Dense submicrometre alumina polycrystals exhibit an increased hardness,[1] wear resistance[2] and strength,[3] but the grain size influence in the fracture toughness K_{Ic} is small in the range $< 5\,\mu m$.[3] For a number of different microstructures the measurement of K_{Ic} by an indentation technique revealed averages of 3·5–4·1 MPa$\sqrt{m}$ with only small influences of grain size, residual porosity, and grain shape.[4] Fig. 1 restores and completes some previous results, and Fig. 2 demonstrates very different shapes of the crystallites in the microstructures. All three materials had been produced by sol–gel approaches where eventually occurring non-equiaxed grains develop *in situ* on sintering. In other microstructures produced by approaches that restrict the possibility to minimize neighbour distances (e.g. *mixing* a powder with platelets), grain shape effects in the toughness may be small.[5] For ceramics, however, that contain *in situ* grown platelets with arbitrary orientation and an aspect ratio of about 10 (Fig. 1(b)) theoretical considerations predict an increase in K_{Ic} of about 70% if the volume fraction of the platelets is 10–15% or more.[6] Two features in Figs 1 and 2 are in sharp contrast with such expectations:

- *Similar* toughness results were obtained for very different shapes: alumina (A) exhibits a more uniform grain shape, ceramic (B) a high concentration of well-defined platelets. These K_{Ic} for ceramic (B) agree perfectly with data published by the producer.[7] Additional hot-isostatic pressing showed that the toughness was not affected by residual porosity.
- On the contrary, ceramic (C) obviously exhibits a lower degree of shape anisotropy as material (B), but its toughness distribution *starts* at about 4 MPa$\sqrt{m}$ which is the *upper* limit of K_{Ic} distributions in known sintered aluminas. The microstructure (C) is somewhat coarser than the examples (A) and (B), yet it is fine-grained enough to exclude any significant *R*-curve behaviour on indentation testing: increasing crack resistance needs stable crack growth for at least some hundreds of micrometers and grain sizes $D \geq 10\,\mu m$, and no *R*-curve was ever observed with grain sizes as small as 1–3 μm.[8,9] Both concentration and aspect ratio of non-equiaxed (rod-like) crystals appear smaller than usually expected for larger toughening effects. Nevertheless, identical testing revealed a toughness distribution that rises up to 6 MPa$\sqrt{m}$ in ceramic (C), whereas common values in the range of 3·5–4 MPa$\sqrt{m}$ were measured for all other investigated aluminas.[3,4]

Both features indicate a shape effect in K_{Ic} that in these very fine-grained ceramics may be different to known models. For example, a large aspect ratio

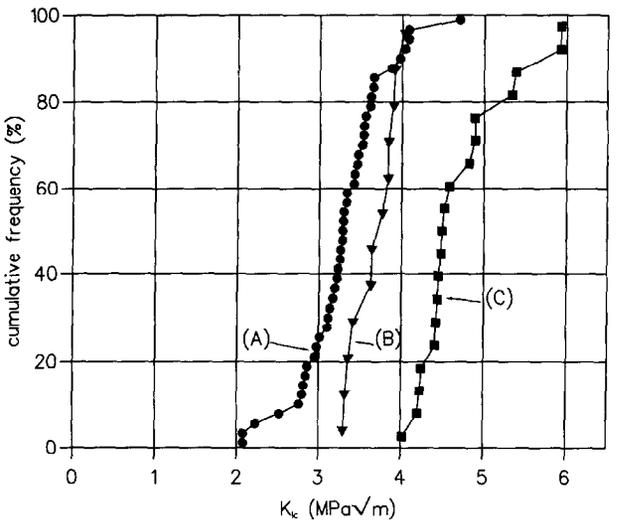

Fig. 1. Fracture toughness distributions of three alumina microstructures (A), (B), and (C) (see Fig. 2) determined by indentation testing.[4]

in ceramic (B) can be insufficient to initiate strong toughness effects if the *absolute* amount of the distortion of the crack path is small due to small grain sizes. On the other hand, it is not certain whether microstructure (A) is close enough to an equiaxed character to exclude *all* shape-depending toughening. Obviously, any explanation will need first a quantitative characterization of observed shapes—which proves difficult for small aspect ratios. After 10 years of intense research with strongly non-equiaxed Si_3N_4 and SiC microstructures, methods exist to describe rod-like or disk-shaped grains with *large* aspect ratios. Of course, available methods have been used to characterize oxide ceramics as well, but little has been done to describe more uniform shapes like those exemplified by Fig. 2(a) and/or by the majority of grains in Fig. 2(c). For example, Koyama and Niihara claim a mechanism to form platelet-shaped alumina grains and prepare microstructures they call 'platelet-shaped' and 'equiaxed', but nothing is said about a criterion to assign a grain to the one or the other group.[10] Similarly, Horn and Messing determine the average size of anisotropic grains in TiO_2-doped alumina from the ratio of the number 'of these grains' per unit area—without defining *which* grains are regarded as anisotropic and are incorporated into this procedure.[11] In fact, to answer this question was simple for their microstructures with very elongated grains accompanied by others that were fairly uniform. A quantitative shape characterization in more homogeneous microstructures as in Figs 2(a) and (c) with their very different toughness data in Fig. 1 needs, however, a more detailed investigation of methods to distinguish equiaxed and non-equiaxed microstructures.

It cannot be the aim of the present work to derive alternative toughening models for the new generation of non-transforming submicrometre ceramics, nor shall we discuss in detail correlations of technological approaches with resulting microstructures. Instead, it is an objective of the

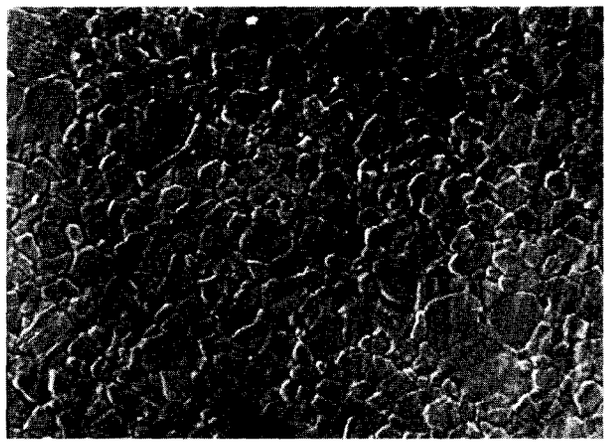

(a)

(b)

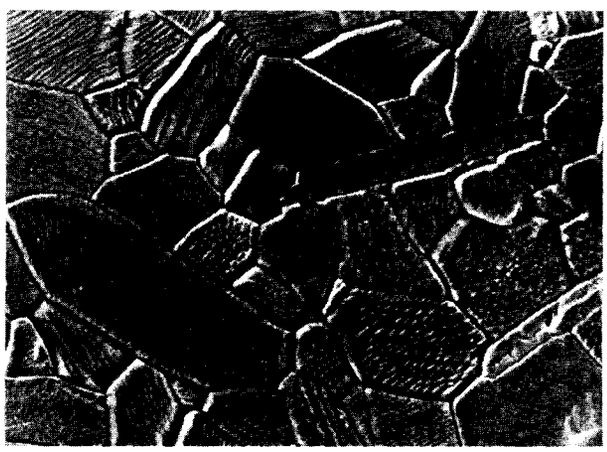

(c)

Fig. 2. Sol/gel-derived sintered Al_2O_3 (thermally etched surfaces): (a) Commercial product (A), SG, Saint Gobin / Norton, Worcester (MA), USA; average grain size D = 0·38 μm (equivalent circle diameter, *area* based mean value), (b) commercial product (B), Cubitron, Minnesota Mining and Manufacturing Co., Saint Paul (MN), USA; average diameter and thickness of the platelets are about 1 μm and 0·05–0·1 μm (c) Ceramic (C) doped with Ce/Ca/Mg (altogether ≤0·5%); D = 1·56 μm.

paper to present a computer-aided procedure that sensitively and on a quantitative basis describes deviations from equiaxed grain shapes in microstructures where anisotropic grain growth resulted in crystals with rather small aspect ratios.

2 Procedures to Analyse Shapes with Small Aspect Ratios

Staehler *et al.* characterized fine-grained sintered alumina by a shape parameter

$$\Phi = 4\pi A/P^2 \tag{1}$$

that 'represents the extent to which each grain deviates from a perfect circle'.[12] In the cross-sectional image, P is the perimeter and A the area of the crystallite. For more than 60 years the reciprocal $1/\Phi$ has been called 'roundness', but Serra[13] indicated that the ratio $P^2/4\pi A$ principally confuses roundness and circularity. Both Φ and $1/\Phi$ give one for the circle. For long crystallites Φ approaches zero whereas the roundness tends to infinity. The latter behaviour of $1/\Phi$ makes the name 'roundness' absurd but offers the advantage of a *large* parameter of shape-anisotropy for crystals with *large* aspect ratios. A more fundamental problem becomes obvious if one considers a circular cog-wheel where the roundness tends to infinity when the number of small cogs increases indefinitely (making the shape increasingly similar to a circle!). Serra has pointed out that the problem is caused by the introduction of a semicontinuous functional (the perimeter) in a shape parameter.[13] However, the consequences for experimental analyses remain small for microstructures where micro-serrated grain boundaries do not occur. And, on the other hand, in a systematic investigation of a number of parameters for defined equiaxed shapes Underwood demonstrated the significant advantage of just $1/\Phi$ for discriminating between different shapes.[14]

In quantitative stereology it is a commonly accepted opinion that the 3-dimensional shape cannot be approached by measurements in a plane (at least not without additional information about size and shape distributions). The one known procedure that overcomes this difficulty makes use of properties of equiaxed bodies and goes back to a Russian work published more than 20 years ago by Saltykov who distinguished three groups of shapes:[15]

- *Equiaxed* bodies meet the necessary and sufficient condition that 'the diameter is (in the average) uniform in all directions or, what is the same, no diameter in anyone dimension or in two selected dimensions predominates compared with the other dimension(s)'.
- *Platelets*
- *Rod-like* bodies.

Saltykov described the deviation of equiaxed convex polyhedra (and only of these!) from a sphere by a 3-dimensional shape parameter with V as the volume and S as the surface:

$$\Phi_3 = 6\sqrt{(36\pi)} \cdot V^{1/3}/S^{1/2} \tag{2}$$

Examples are given in Table 1 and have been used by Saltykov to derive a generally valid condition (not restricted to any special forms) for convex equiaxed polyhedra:

$$0{\cdot}8 \leq \Phi_3 \leq 1{\cdot}0 \tag{2(a)}$$

Note that (2(a)) represents a necessary but not sufficient condition: anisotropically grown crystals with a shape close to a sphere (e.g. ellipsoids with small aspect ratios) are *non*-equiaxed but exhibit, nevertheless, Φ_3 values close to one. On the other hand, with Saltykov's statement that 'for both non-equiaxed and concave bodies the value (of Φ_3) is considerably less' (than 0·8), an equiaxed shape can be reliably excluded if the condition (2(a)) is not met. Hence, the sufficient (not necessary) condition is for *non*-equiaxed polyhedra:

$$\Phi_3 < 0{\cdot}8 \tag{2(b)}$$

Two implications are important. First, the data in Table 1 and the associated conditions (2(a),(b)) result from general geometrical consideration and

Table 1. Saltykov's parameters for examples of equiaxed shapes

Φ_3 *for 3-dimensional bodies*	*Polyheders*		*Polygons*	Φ_2 *for 2-dimensional shapes*
1·00	Sphere	—	Circle	1·00
		(number of facets → infinity)		
0·95	Tetrakaidecahedron	—	Hexagon	0·95
0·92	Octahedron		—	—
0·90	Cube	—	Square	0·89
0·82	Tetrahedron	—	Triangle (equilateral)	0·78
		(minimum number of facets)		

have to be modified if in special materials individual shapes do *not* occur. Second, Saltykov's approach presents the unique chance to derive a further relationship for the analysis of practically important *two*-dimensional cross-sections *without* the need of introducing additional information about the (*a priori* unknown) shapes. To achieve this, Saltykov defined a 2-dimensional shape parameter

$$\Phi_2 = 2\sqrt{(\pi A)}/P \qquad (3)$$

to characterize 2-dimensional (equiaxed) polygons; the same symbols are used as in eqn (1) to show the equivalence $\Phi = \Phi_2^2$ ('roundness' $= 1/\Phi_2^2$). To associate statistically Φ_2 of cross-sectional shapes with Φ_3 of the 3-dimensional body, the *average* $\overline{\Phi}_2$ of arbitrary sections has to be compared with the (one) Φ_3-parameter of the body. Saltykov demonstrated that in the special case of convex, equiaxed bodies the following features apply:

- Sectioning gives an angle α_2 in the cross-section that, depending on the orientation, can be smaller or larger than the *spatial* angle α_3 included by the adjacent facets.
- For arbitrary sections, the probability of the plane angle α_2 exhibits a maximum at a value close to α_3, and the average α_2 equals the average of α_3. Saltykov's conclusion was: the statistically 'average shape of the plain section is a uniform polygon with an inner angle (at one of its apexes) that equals the average angle between the facets of the body' (α_3). For example, the 'average shape' of cross-sections through a cube ($\alpha_3 = 90°$) is a square, for the tetrakaidecahedron ($\alpha_3 = 120°$) it is a hexagon (imaginary values result for bodies where the average α_3, does not coincide with the angle of a regular polygon).
- Hence, the bodies are associated with 2-dimensional polygons (Table 1). The similarity of Φ_2 and Φ_3 values for these pairs of 2- and 3-dimensional shapes throughout the whole equiaxed range gives evidence for Saltykov's conclusion: the *average* value of Φ_2, determined for a sufficiently large number of crystals in a *plain* section of a microstructure, equals Φ_3 and characterizes the average *3-dimensional* shape of the crystallites.

Therefore, in analyses of sectioned microstructures the necessary condition for equiaxed (three-dimensional!) particles and the sufficient condition for non-equiaxed particles are:

$$\text{equiaxed particles}: 0{\cdot}8 \leq \overline{\Phi}_2 \leq 1{\cdot}0 \qquad (3(a))$$

$$\text{non-equiaxed particles}: \overline{\Phi}_2 < 0{\cdot}8 \qquad (3(b))$$

where $\overline{\Phi}_2$ is the arithmetic average of all individual Φ_2 determined on the cross-section according to eqn (3). It is important to emphasize that the relationships (2(b)) and (3(b)) are sufficient conditions to identify non-equiaxed shapes, but the parameter $\overline{\Phi}_2$ must not be used to quantify the degree of anisotropy of non-equiaxed particles (due to the restriction to equiaxed shapes at some points of the above reasoning).

It was an objective of the present work to apply Saltykov's parameter $\overline{\Phi}_2$ to a wide range of advanced microstructures that became available recently with average grain sizes of 0·2–2 μm. The comparison with other form factors that additionally describe the *degree* of anisotropy in the growth of non-equiaxed grains is intended to show which approach is best to distinguish different shapes with small aspect ratios. Microstructures prepared by different technologies and with different doping additives were included to give a first indication whether some of these techniques may be more or less adequate to produce selected crystal shapes.

All form factors to assess anisotropy are introduced here in a way that gives a value of one for the circle and increasing results for rising deviations from the equiaxed shape. All of the following factors are less sensitive to image noise than Φ, $1/\Phi$ and $\overline{\Phi}_2$ because they avoid the use of semi-continuous functionals criticized by Serra.[13] Contrary to $\overline{\Phi}_2$ they describe the *apparent* shape of the plain images only, and any more reliable information about the true shape of 3-dimensional crystals needs additional assumptions that have to be introduced into the analysis.

For elongated shapes the average of the (apparent) aspect ratio

$$R = L_{max}/L_{min} \qquad (4)$$

is smaller than the value of the 3-dimensional body. L_{max} and L_{min} are the maximum length and minimum width of the cross-section measured without any orientational relationship between the two directions. A problem in uniform microstructures is that even exactly equiaxed polygons give values remarkably different of one. The maximum is $R = 1{\cdot}41$ for the square, and non-equiaxed sections have to exhibit an aspect ratio of *more* than 1·41 to be distinguished from the parameter range associated with both equiaxed and non-equiaxed shapes which exhibit R values of 1·00–1·41. Therefore, the *necessary* condition for equiaxed shapes and the *sufficient* condition for non-equiaxed cross-sections are:

$$\text{equiaxed particles} : 1{\cdot}0 \leq R \leq 1{\cdot}41 \qquad (4(a))$$

$$\text{non} - \text{equiaxed particles} : 1{\cdot}41 < R \qquad (4(b))$$

The problem of a rather wide range 1·00–1·41 where equiaxed and non-equiaxed shapes cannot be distinguished is reduced if a relationship between the two directions required for the determination of an aspect ratio is fixed, e.g. by defining

$$R_{orth} = L_{max}/L_{orth} \qquad (5)$$

with L_{orth} as the apparent width of the section measured orthogonal to the direction of L_{max}. Here the hexagon exhibits the largest value of all equiaxed polygons ($R_{orth} = 1{\cdot}15$). This value is close to one and makes the range small where data of both equiaxed and non-equiaxed shapes coexist. Hence, the necessary condition for equiaxed shapes and the sufficient condition for non-equiaxed cross-sections are:

$$\text{equiaxed particles} : 1{\cdot}0 \leq R_{orth} \leq 1{\cdot}15 \qquad (5(a))$$

$$\text{non} - \text{equiaxed particles} : 1{\cdot}15 < R_{orth} \qquad (5(b))$$

Another shortcoming of R is the strong influence of arbitrary (often short) deviations of the perimeter from a 'rounded' contour, deviations that cause more extreme values of L_{max} *and* L_{min} than are actually typical for the given shape as a whole. The result is an exaggerated result for the derived aspect ratio. To reduce this difficulty, one can measure the whole cross-sectional area A instead of L_{min} and define another form factor as

$$R_A = (\pi/4) \cdot (L_{max}^2/A) \qquad (6)$$

With its dependence on a unit like the area and considering the discussion given by Serra,[13] R_A is a measure less sensitive to image noise than R and R_{orth}. Unfortunately, it discriminates less between equiaxed and non-equiaxed polygons due to exceptionally high values for some of the equiaxed shapes: $R_A = 1{\cdot}81$ for the equilateral triangle, and $R_A = 1{\cdot}57$ for the square.

The triangle, however, needs separate consideration. Contrary to fundamental work like the definition of new parameters by Saltykov that should not depend on special characteristics of a material, the application in ceramographic analyses has to take into account that not all generally imaginable shapes occur. For sintered alumina it has been well-known for a long time that crystals with very small numbers of facets (like the tetrahedron) are not developed. Instead, polyfaceted shapes are typical, and Coble used the tetrakaidecahedron for his model of sintering.[16] With such polyfaceted bodies, the probability of triangular plain sections should be small, in fact, in micrographs of alumina as in most other ceramics triangular shapes are rarely observed. Hence, among practically important equiaxed polygons it is not the triangle but the square that exhibits the largest $R_A = 1{\cdot}57$, and the necessary condition for equiaxed shapes and the sufficient condition for non-equiaxed cross-sections become

$$\text{equiaxed particles} : 1{\cdot}0 \leq R_A \leq 1{\cdot}57 \qquad (6(a))$$

$$\text{non} - \text{equiaxed particles} : 1{\cdot}57 < R_A \qquad (6(b))$$

Another consequence seems even more important: the conditions (2(a),(b)) and (3(a),(b)) used to discriminate equiaxed and non-equiaxed shapes by Saltykov's parameters become much more stringent if in Table 1 instead of the triangle, the cube (with $\Phi_3 = 0{\cdot}90$ and $\Phi_2 = 0{\cdot}89$) is considered that equiaxed body (really existing in the microstructure) which deviates most from the sphere. Actually, even cube-like crystals are rare, a feature that shifts the limit excluding equiaxed characters to values of slightly more than 0·90. For the present analysis it was assumed, however, that with Table 1 and the general experience of occurring shapes in Al_2O_3 microstructures, reliable conditions to distinguish the two groups of crystal shapes are

$$\text{equiaxed particles} : 0{\cdot}9 \leq \overline{\Phi}_2 \leq 1{\cdot}0 \qquad (3(c))$$

$$\text{non} - \text{equiaxed particles} : \overline{\Phi}_2 < 0{\cdot}9 \qquad (3(d))$$

where the same conditions hold for Φ_3 as well.

Table 2 lists the form factors used to characterize the shape of non-equiaxed sections. The preceding introduction of these parameters has shown that there is a range between one and an upper limit $(1 + B_{equ})$ associated with both equiaxed and (slightly anisotropic) non-equiaxed cross-sectional shapes. For some form factor, $(1 + B_{equ})$ is given by that equiaxed shape which exhibits the largest value. For the aspect ratio R it is the square that gives $(1 + B_{equ}) = 1{\cdot}41$ and a width $B_{equ} = 0{\cdot}41$ of the ambiguous parameter range. B_{equ} should be small if equiaxed and non-equiaxed shapes are discriminated more precisely, but such an advantage may be useless if it is achieved at the expense of a

Table 2. Parameters used to characterize microstructural shapes generated by anistropic grain growth. See text for explication of B_{equ} and X_{dis}

Parameter	*Range with values originating from both equiaxed and (slightly antistropic) non-equiaxed shapes*	B_{equ}	*Values of parameters for elongated shapes with an axis ratio a/b = 2.* *Ellipse*	*Rectangle*	X_{dis} *for Ellipse/Rectangle*
$R = L_{max}/L_{min}$	1–1·41	0·41	2	2·24	2·0/1·4
$R_{orth} = L_{max}/L_{orth}$	1–1·15	0·15	2	1·25	0·7/5·7
$R_A = (\pi/4)\cdot(L_{max}^2/A)$	1–1·57	0·57	2	1·96	0·7/0·8

factor's sensitivity to anisotropy. For the latter objective, the difference D_{equ} between $(1 + B_{equ})$ and the actual (higher) parameter value of a non-equiaxed shape should be large. For example, with $(1 + B_{equ}) = 1{\cdot}15$ close to one, R_{orth} shows a favourably small $B_{equ} = 0{\cdot}15$ (Table 2)—but for a rectangle with an axis ratio of 2 the value $R_{orth} = 1{\cdot}25$ is also very small. Here, the difference D_{equ} between this value and $(1 + B_{equ}) = 1{\cdot}15$ is only 0·10 (8% related to the actual value of R_{orth}). The objective of large D_{equ} with small B_{equ} is described in Table 2 by high ratios $X_{dis} = D_{equ}/B_{equ}$ (given for one 'round' and one faceted example: an ellipse and a rectangle). As a result, it turns out that it is R_{orth} which exhibits an exceptionally high sensitivity to distinguish *faceted* slightly non-equiaxed sections from equiaxed shapes. For shapes with a more *rounded* character, however, a high X_{dis} for the ellipse suggests the best behaviour for the aspect ratio R. R_A may be expected the least reliable to discriminate between equiaxed and non-equiaxed cross-sectional shapes. However, the estimator X_{dis} used in Table 2 to evaluate the parameter properties depends on the actual shape of the analysed sections. It was, therefore, an objective of the present work experimentally to compare the different behaviour of all anisotropy parameters for real alumina microstructures.

The ranges given for Saltykov's parameter $\overline{\Phi}_2$ by the relationship (3(c)) and for the anisotropy parameters (form factors) by $1-(1 + B_{equ})$ in Table 2 are representative for equiaxed shape and additionally for non-equiaxed shapes with aspect ratios close to unity. Therefore, a reliable identification of non-equiaxed forms is possible only outside these parameter ranges—where, however, it can never comprise *all* non-equiaxed individuals. Hence, any identification of non-equiaxed shapes outside the ambiguous range will be conservative, be it performed with Saltykov's parameter $\overline{\Phi}_2$ and criterion (3(d)) or by use of the anisotropy parameters and the criteria (4(a),(b)), (5(a),(b)), and (6(a),(b)) repeated in the second column in Table 2. The real amount of non-equiaxed grains will always be somewhat higher than given by the results of the above procedures which overestimate the equiaxed character.

3 Experimental Procedure

With the exception of the microstructures (A)–(C) (Fig. 2) all other ceramics were prepared in our laboratory. The preparation and mechanical characterization of pressureless sintered alumina microstructures with average grain sizes between 0·2 and 2 μm by sol–gel[4] or by powder technological approaches,[3] respectively, have been described previously. Typically, today's boehmite used as raw material for sol–gel alumina contains 0·2–0·4% TiO_2 known to promote anisotropic grain growth on sintering.[11] Aside from this impurity, all ceramics investigated here are 'pure' Al_2O_3 in the sense that they contain less than 0·5 wt% of MgO or other additives if not stated otherwise. Carefully ground and polished cross sections were investigated after thermal etching for 1 h at temperatures that usually were at least 50 K lower than the sintering temperatures. Additional information about the grain size without the superimposed effect of etching was obtained by investigating fracture surfaces, and both plain microfaces in subregions with a high percentage of intragranular fracture and internal surfaces of pores ('etched' on sintering) confirmed the data derived from thermally etched cross-sections within limits of ± 10%.

In usual scanning electron micrographs (Fig. 2), the local brightness of the thermally etched crystallites and the grain boundary contrast are rather inhomogeneous, which makes a completely automatic analysis impossible and requires an interactive image reconstruction. The maximum and orthogonal Feret diameter L_{max} and L_{orth}, the perimeter P and the area A were then determined using the Quantimet 570 image analysis system (Leica, Germany). About 1000 crystals were used to determine the average grain size (equivalent circle diameter, *area*-based mean value), the arithmetic mean of Saltykov's parameter Φ_2 (required by the mathematical procedure that correlates this average with the 3-dimensional characteristics as outlined above), and area-weighed means of other form factors which characterize the degree of anisotropic grain growth. *Mean* values characterize the average grain size throughout this paper; *median* values of the distributions are smaller by about 2–15%.

Considering the previously-demonstrated equivalence of Saltykov's Φ_2 with Φ according to eqn (1) and with the so called 'roundness', neither Φ nor the roundness have been measured here.

4 Results

Fig. 3 shows digitalized micrographs of two 'pure' (essentially single-phase) alumina samples representing more elongated and more uniform crystals, respectively. Table 3 gives the results of the quantitative analyses. Sample notations SG point to sol–gel derived ceramics, specimens called PD had been prepared by powder technological approaches.

In agreement with the subjective optical impression represented by the micrograph (Fig. 3(a)). in material SG1 the anisotropy parameter R_{orth} and all other tested form factors clearly reveal a strongly non-equiaxed character of the analysed cross-sectional shapes (Table 3). Saltykov's $\overline{\Phi}_2$ indicates the same for the sections and for the 3-dimensional microstructure. For the present case it is, therefore, obvious that either the anisotropy parameters R, R_{orth} and R_A give a valid characterization of a 3-dimensional anisotropy.

Much more remarkable are the results for the submicrometre sample PD1 in Fig. 3(b). It is not surprising that the marked concentration of equiaxed grains is considerably higher than observed in SG1 (Fig. 3(a)). However, even in this—apparently very uniform—microstructure the average value of R_{orth} indicates a majority of anisotropically grown crystals (Table 3). R, R_A and Φ_2 exhibit averages just at the limit of the parameter range for only non-equiaxed shapes, but remembering the *conservative* character of these criteria that can never identify all anisotropic particles it is obvious that even in this uniform microstructure *all* of the investigated parameters give evidence of a non-equiaxed character of a majority of crystals.

Of course, to reject an equiaxed characterization of sample PD1 does not mean to deny its nevertheless uniform substance. Because of this uniform microstructure PD1 was selected for further tests of the different sensitivity of anisotropy parameters. Figures 4 and 5 give the same part of the microstructure as in Fig. 3(b), but now the aspect ratio R and the form factor R_A discriminate equiaxed and non-equiaxed sections. With the *different* criteria (4(a),(b)), (5(a),(b)), and (6(a),(b)) discriminating equiaxed and non-equiaxed shapes by means of different form factors, different widths of classes have to be applied to mark equally shaped crystals of the one microstructure in Figs 3(b), 4(a), and 5(a) (*one* approximated criterion $< 1{\cdot}5$ was used in Figs 4(a) and 5(a)). In Figs 3,

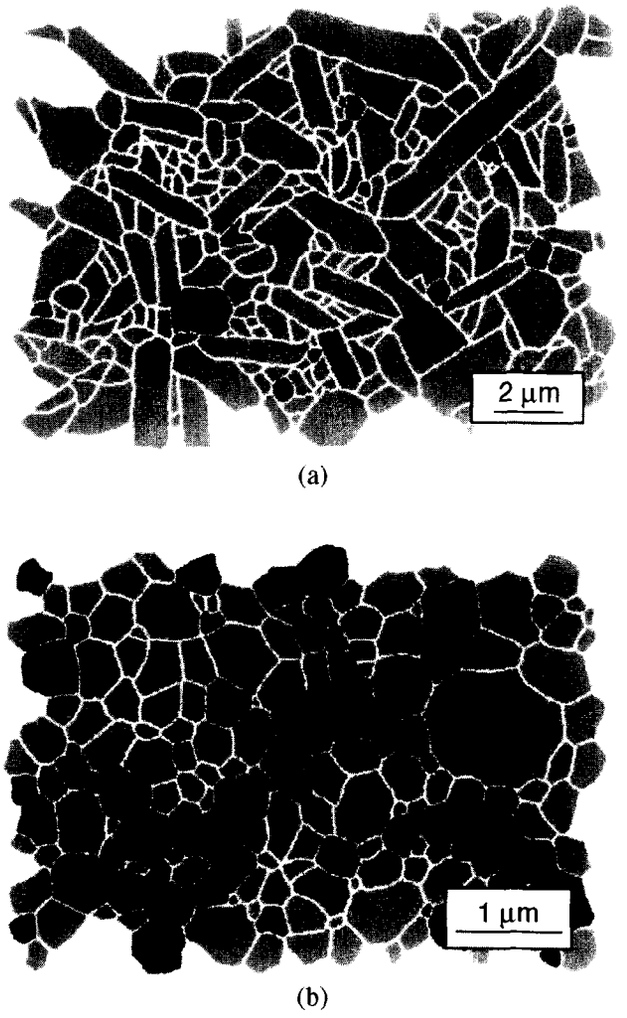

Fig. 3. Digitalized micrographs of alumina microstructures with more elongated shapes (Fig. 3(a): sample SG1) and with a more uniform character (Fig. 3(b): sample PD1). Marked crystals comprise equiaxed shapes and non-equiaxed shapes with very small aspect ratios (form factor $1 \leq R_{orth} < 1{\cdot}15$). All unmarked crystals are non-equiaxed.

Table 3. Results of the quantitative analyses for microstructures SG1 (Fig. 3(a)) and PD1 (Fig. 3(b)). D is the average grain size

Microstructure code- D(µm)	*Criteria for non-equiaxed shapes*			
	$\overline{\Phi}_2$ *(Saltykov) (arithmetical average)*	R	R_{orth} *(area-weighed averages)*	R_A
	$\overline{\Phi}_2 < 0{\cdot}90$	$R > 1{\cdot}41$	$R_{orth} > 1{\cdot}15$	$R_A > 1{\cdot}57$
SG1 – 1·72	0·80	2·40	2·09	2·72
PD1 – 0·42	0·90	1·39	1·28	1·58

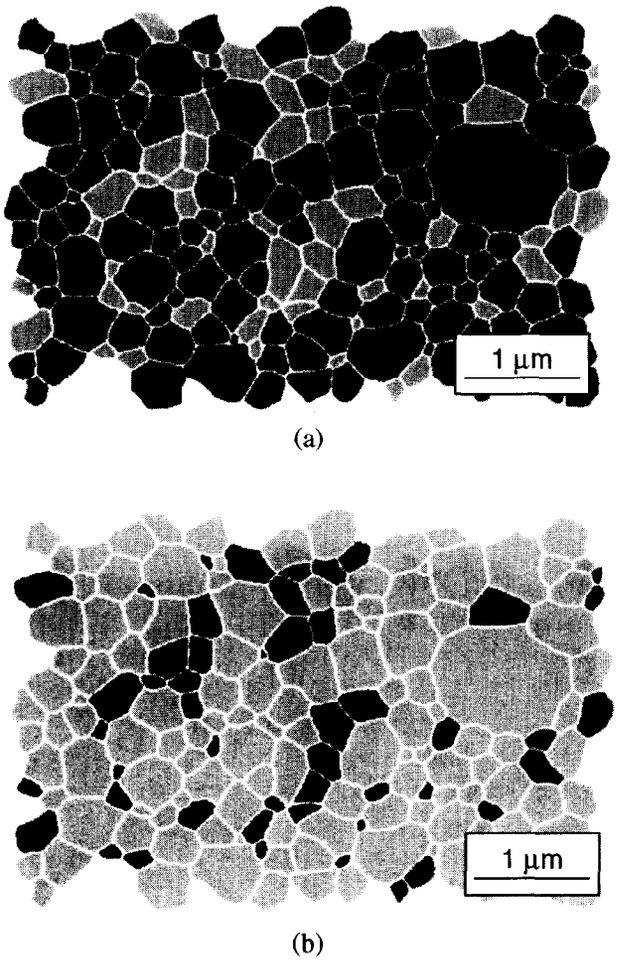

Fig. 4. Digitalized micrograph of the uniform alumina microstructure PD1 analysed by the aspect ratio R. Figure 4(a) marks *all* shapes with $1 \leq R < 1{\cdot}5$ (equiaxed *and* non-equiaxed; all unmarked grains are *non*-equiaxed with $R > 1{\cdot}5$). In Fig. 4(b) non-equiaxed sections with *small* anisotropy $1{\cdot}5 \leq R < 2$ are marked.

4(a), and 5(a) all unmarked crystals meet the (sufficient) criterion for non-equiaxed shapes. To demonstrate graphically the (small) degree of anisotropy sufficient for a reliable classification as 'non-equiaxed' by R and R_A (just beyond the limit of 1·5), Figs 4(b) and 5(b) mark non-equiaxed grains with parameter values 1·5–2·0.

Comparing the result obtained in Fig. 3(b) by the form factor R_{orth} with the performance of R and R_A in Figs 4(a) and 5(a), the latter are much less sensitive in recognizing non-equiaxed shapes with small aspect ratios: in Figs 4(a) and 5(a) considerably more crystals are associated with the lowest class that contains an ensemble of both equiaxed and non-equiaxed individuals (here with parameter values < 1·5). Contrary to the estimator X_{dis} in Table 2, this disadvantage is expressed even more in R (Fig. 4(a)) than in R_A (Fig. 5(a)).

With Figs 3(b), 4 and 5 and with Table 3, R_{orth} is established as the anisotropy parameter that distinguishes best equiaxed shapes and anisotropic forms with small aspect ratios. On the other hand, the 'usual' aspect ratio R gives a more direct idea of the apparent elongation of anisotropically grown crystals. Therefore, the comparative analysis of 20 different alumina microstructures with relative densities > 99% and average grain sizes in the range 0·2–2 μm was performed with the mean grain size and the mean (apparent) aspect ratio R as parameters of a general characterization, whereas the test for the equiaxed character was performed with Saltykov's parameter $\overline{\Phi}_2$, and R_{orth} was used to assess the *degree* by which microstructures deviate from an equiaxed character.

Table 4 classifies observed types of microstructures. Actually, 20 different microstructures are insufficient to get ultimately significant data for each group of a detailed classification, and Table 4 indicates preliminary trends only. Nevertheless, some interesting results are obvious:

- Like PD1 (Figs 3(b), 4, 5, Table 3), many microstructures are quite uniform and *approach* the range of $\overline{\Phi}_2$ associated with equiaxed microstructures; this applies for both

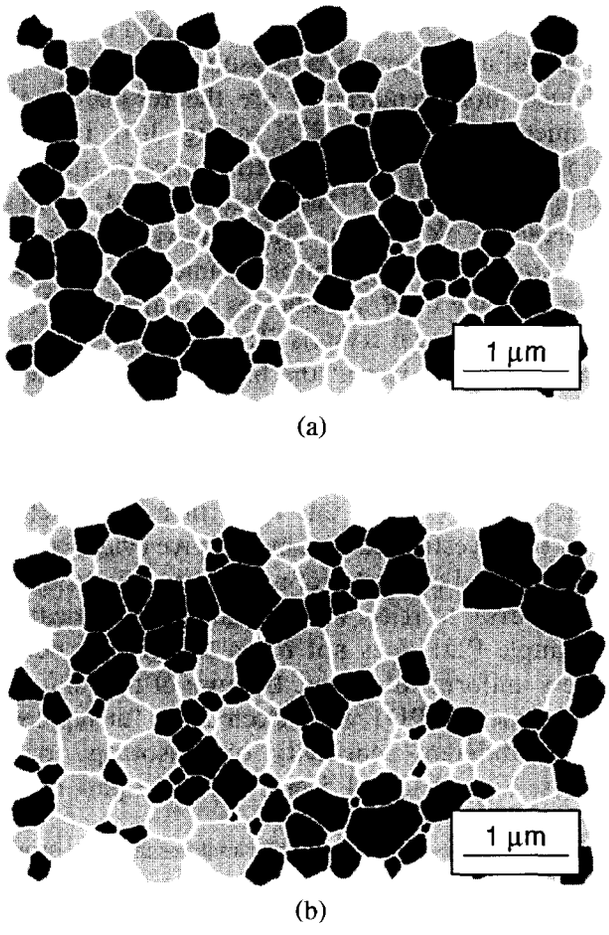

Fig. 5. Digitalized micrograph of the uniform alumina microstructure PD1 analysed by the form factor R_A Figure 5(a) marks *all* shapes with $1 \leq R_A 1{\cdot}5$ (equiaxed and non-equiaxed; all unmarked grains are *non*-equiaxed with $R_A > 1{\cdot}5$). In Fig. 5(b) non-equiaxed sections with *small* anisotropy $1{\cdot}5 \leq R_A < 2$ are marked.

Table 4. Shape characterization for different types of fine-grained alumina microstructures depending on grain size and processing. Two individual microstructures from Figs 2(a) and 2(c) are included for comparative purposes

Microstructure	*Average aspect ratio*	$\overline{\Phi}_2$ *(Saltykov) (arithmetical average)*	R_{orth} *(area-weighed averages)*
	R	*Criteria for non-equiaxed shapes*	
		$\overline{\Phi}_2 < 0.90$	$R_{orth} > 1.15$
Submicrometre sintered alumina (grain sizes 0·2–0·8 μm)			
→Powder technological approaches			
(a) more uniform microstructures	≈1·4	0·89–0·90	≈1·3
(b) more anisotropic samples		(no anisotropic microstructures could be found!)	
→ Sol–gel derived microstructures			
(a) more uniform microstructures	1·4–1·5	0·87–0·90	1·3–1·4
(b) more anisotropic samples	≈1·8	≈0·87	≈1·65
Sintered alumina with grain sizes 0·9–2 μm			
→Powder technological approaches			
(a) more uniform microstructures	≈1·4	≈0·89	≈1·3
(b) more anisotropic samples	≈2·0	≈0·87	≈1·85
→Sol/gel derived microstructures			
(a) more uniform microstructures	≈1·4	0·86–0·90	1·3–1·4
(b) more anisotropic samples	2·1–2·4	0·80–0·83	2·0–2·1
Sol–gel-derived microstructures from Fig. 2			
Uniform sample (A) grain size 0·38 μm	1·51	0·89	1·40
Sample (C), grain size 1·56 μm	2·03	0·84	1·83

grain size ranges and independent of the way the samples have been produced. However, *no one* of the investigated microstructures is really equiaxed. Figure 6 illustrates this phenomenon graphically. Note the large distance between the smallest R_{orth} values of even most uniform microstructures and the parameter range that includes equiaxed shapes.

- The investigated powder approaches included a batch with additives suggested to promote strongly anisotropic grain growth:[17] + 2% SrO/ + 1·8% Cr_2O_3(+ 25% ZrO_2) (all data are wt%). In fact, with a submicrometre grain size of 0·85 μm, this specimen showed the strongest anisotropy of all powder-derived microstructures (aspect ratio $R = 2 \cdot 0$, $\overline{\Phi}_2 = 0{\cdot}85$, $R_{orth} = 1{\cdot}83$)—but an even more developed anisotropy was observed in the sol–gel-derived sample SG1 with no other doping as 0·5% MgO (Fig. 3(a), Table 3). This phenomenon is not unique in these two batches: Table 4 indicates a stronger anisotropy of grain growth as a common phenomenon in *all* sol–gel derived groups.
- With the exception of the group with the coarsest, most anisotropic sol–gel-derived samples, Table 4 shows that similar aspect ratios and similar average values of Φ_2 and R_{orth} can be associated with submicrometre and larger grain sizes. Within the range of microstructures investigated here that means:

1. Independent of the applied technology, fairly uniform microstructures can be produced also with larger grain sizes. This applies even for sol–gel-derived microstructures (with a TiO_2-impurity) doped with 0·1% Y_2O_3 which is also assumed to promote anisotropic grain growth (the effect is somewhat reduced when Y_2O_3 is added together with MgO).[18]
2. On the other hand, a proper approach can induce a significant anisotropy with limited grain growth, i.e. at small submicrometre grain sizes. However, with Table 4 this behaviour seems restricted to sol–gel samples, and even this technology usually requires more complex additives to obtain large aspect ratios $R > 5$. Figure 2(b) shows a commercial example (doped with MgO, Y_2O_3, La_2O_3, and possibly Nd_2O_3).[19]

To compare grain shape parameters with previous toughness results, the average form factors were determined for those two materials in Fig. 1 that exhibited a toughness at the lower bound of the conventional data range (A) and the highest toughness ever reported for a fine-grained alumina (C), respectively. Table 4 compares these individual results with the typical shape characteristics obtained for the different types of sintered Al_2O_3 microstructures. Sample (A) belongs to the group of submicrometre sol–gel-derived aluminas with more uniform microstructures. In spite of the really uniform appearance (Fig. 2(a)) the quantitative assessment, however, shows that it is one of the *least* uniform representatives of this type and not equiaxed at all. Similarly, within the coarser-grained non-uniform

group sample (C) is one of the least *an*isotropic examples.

Hence, neither microstructure (A) nor (C) associate their very different toughness (Fig. 1) with a uniquely uniform or an exceptionally anisotropic character of their *average* crystal shapes. Assuming that the toughness might be more influenced by the grains with the most anisotropic character, additional information about the distributions of anisotropy parameters were obtained and are presented in Table 5. Unlike the average values of the form factors, the upper limits of the distributions did not show a significant dependence on ceramic processing, and the data for the different types of microstructures in Table 5 are valid for both sol–gel-derived microstructures and samples prepared by powder approaches.

The frequency distribution of form factors in the tough microstructure (C) shows two noteworthy features (Table 5). First, it exhibits the largest upper limits R^{max} and R_{ort}^{max} of the distributions. In contrast, sample (A) shows a microstructure where both R^{max} and R_{ort}^{max} are slightly smaller than typically observed in similar submicrometre and uniform microstructures. However, there is a remarkably small *content* of elongated crystals in (C) exceeding the R^{max} and R_{ort}^{max} values of the uniform microstructure (A) or of sample SG1 (which combines a strong shape anisotropy with a similar grain size as (C)). In the tough material (C) few crystals with large aspect ratios appear embedded in a matrix where more than 90 vol% of the microstructure shows an aspect ratio of less than 3.

The second remarkable feature in the tough microstructure (C) is a bimodal correlation of shape anisotropy and grain growth (Fig. 7): rising anisotropy associated with a growing (apparent) grain length L_{max} is observed for grains larger than about 4 μm, but these grains do not develop the highest aspect ratios, and R_{orth} remains smaller than 3. On the other hand, extreme anisotropy as found in no other investigated microstructures is associated with grains that show an L_{max} close to the average grain size.

5 Discussion

As expected, because of the large value of X_{dis} in Table 2, R_{orth} is the anisotropy parameter that discriminates most sensitively between (i) anisotropically grown crystals with small aspect ratios $R \approx 1{\cdot}5$–2 (and, of course, more strongly anisotropic crystals), and (ii) the group of equiaxed shapes and non-equiaxed grains with very small form factors $R < 1{\cdot}5$. An advantage of the aspect ratio R for 'round' (ellipsoid) shapes as suggested by X_{dis} (Table 2) was not confirmed experimentally, R is even less sensitive than R_A (Figs 4 and 5). It is not clear whether this behaviour is caused by the faceted shapes typical for sintered alumina or, more generally, by the limited accuracy in measuring R as discussed in paragraph 2 of the introduction.

Figures 6 and 3(a) are an experimental justification for the reduction of the 'equiaxed' parameter range for $\overline{\Phi}_2$ and Φ_3 from originally 0·8–1 (eqns (2a) and (3a)) to 0·9–1 (eqn (3c)) associated with the application to sintered ceramic microstructures which do not contain tetrahedral bodies: with a limit of 0·8, Φ_2 would recognize *all* of the examined microstructures as equiaxed (Fig. 6(a))—an obvious absurdity for microstructures such as that shown in Fig. 3(a) and a discrepancy compared to the results of R_{orth} in Fig. 6(b). Note that in Fig. 6(b) the R_{orth}-boundary of the 'equiaxed' range of values does *not* depend on the occurrence of tetrahedra or cubes because $R_{orth} \leq 1{\cdot}15$ holds for

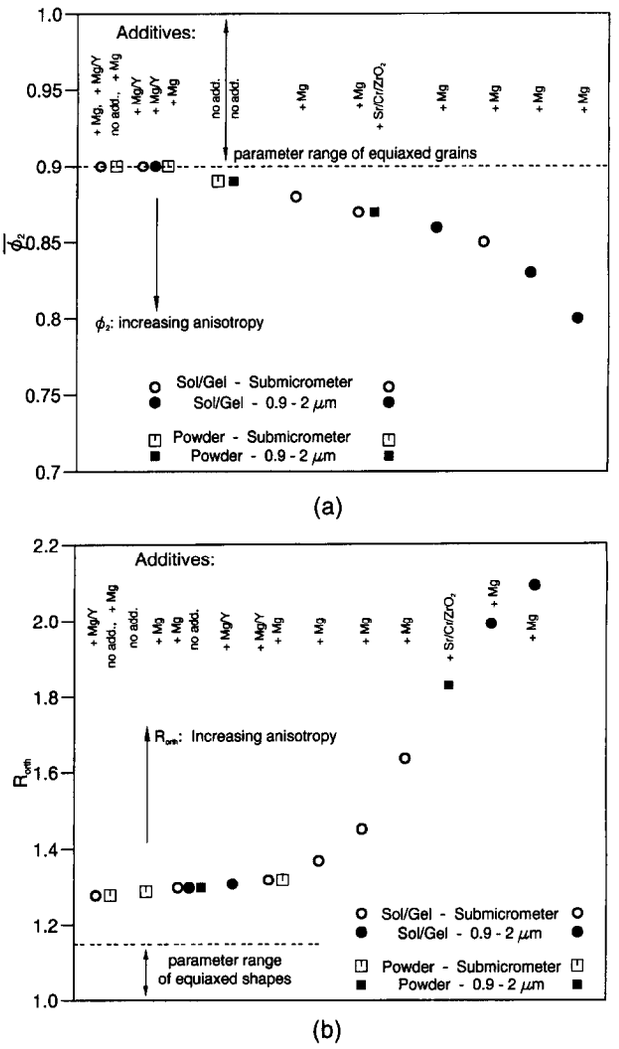

Fig. 6. Ranking of grain shape observations. (a) With Saltykov's parameter, $0{\cdot}9 \leq \overline{\Phi}_2 \leq 1{\cdot}0$ is the necessary condition for an equiaxed character of the analysed bodies, and $\overline{\Phi}_2 < 0{\cdot}9$ indicates non-equiaxed shapes. (b) The anisotropy parameter R_{orth} increasing beyond $R_{orth} = 1{\cdot}15$ means growing anisotropy of non-equiaxed shapes.

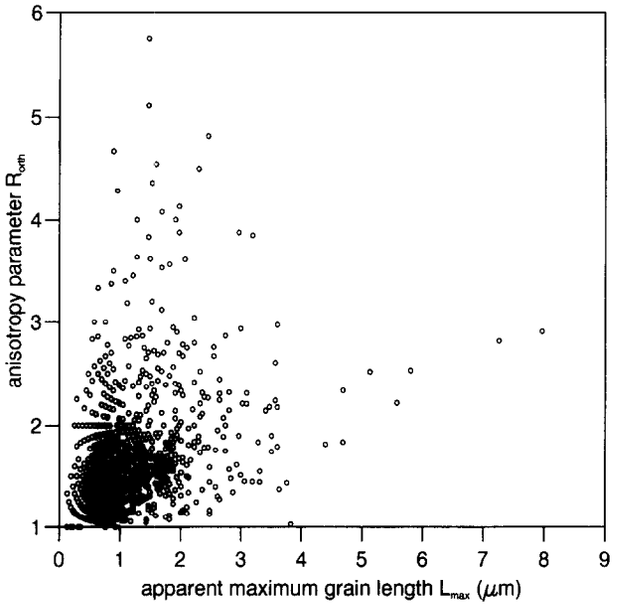

Fig. 7. Correlation of form factor R_{orth} with the apparent maximum length L_{max} of the grains in the tough material (C). Toughness and microstructure cp. Figs 1 and 2(c).

both equilateral triangles and squares, a feature that makes this boundary very reliable independent of special forms of the crystallites.

There is hard experimental evidence supported by all of the investigated parameters that even the most uniform microstructures (e.g. Figs 2(a) or 3(b)) are not equiaxed because a majority of their crystals do not meet the conditions necessary for such a classification. This result is surprising if one regards the literature where (outside of Russia) the term 'equiaxed' has experienced an inflationary use during the past 15 years. Actually, very different microstructures have been called equiaxed without any qualitative or quantitative definition of this expression and without noticing that equiaxed means (exactly) *equal* and not *similar* axes. The verbal definition given by Saltykov 20 years ago is very clear at this point and does not need any comment. It is, therefore, obvious that equiaxed microstructures will be extremely difficult (if not impossible) to prepare, whereas advanced technologies are well able to *approach* this aim by delivering increasingly uniform shapes (Fig. 6).

The average values of form factors indicate more anisotropic grain growth in sol–gel-derived microstructures than in samples prepared by powder approaches (Table 4), but no differences were observed in the upper limits of the distributions, in the observed *range* of shape anisotropy. Hence, the background of the more pronounced anisotropic character in sol–gel-derived samples is not the development of some individual crystals with very large aspect ratios but an increased frequency of *many* non-equiaxed crystals with slight or moderate anisotropy. This behaviour can only in part be explained by TiO_2 impurities in boehmite raw materials suggested to promote anisotropic grain growth.[11] Similar TiO_2 concentrations added to corundum (α-phase) *powders* show much smaller and even contrary effects: it had been reported that 'large grains (of alumina) became nearly spheroidal as the titania content increased beyond about 1%'.[20] A more straightforward explanation of the observed differences between powder approaches and sol–gel-derived alumina is the different amount of grain *growth* on sintering: the grain size of boehmite is 20–40 nm, that of advanced α-powders is 200 nm, and with an average grain size of 0·5 μm in the sintered microstructures the grain growth ratio is about 2·5 in powder approaches but more than 10 in the sol–gel-derived material. Obviously, more growth in non-cubic crystals increases the probability to develop anisotropic shapes. Morphological peculiarities of the boehmite, of formed transitional phases and of added seeds may additionally contribute to the anisotropic character in sol–gel-derived alumina microstructures. It should, however, be emphasized once more that all this discussion refers to the majority of crystals with relatively small aspect ratios. More elongated or platelet-like shapes like those in Figs 2(b) and (c) need complex additives.

On the other hand, fairly uniform microstructures can be produced even with larger grain sizes independent of the technology (Table 4). Hence, grain growth in alumina is not necessarily associated with significant anisotropy. For the sintering of α-phase powders this feature has been known for a long time (since the discovery that small MgO additives avoid exaggerated grain growth), and it is interesting to see here that the same can be achieved in sol–gel materials with large grain growth ratios of more than 10, under appropriate conditions.

As to the extremely tough material (C) (Fig. 2(c)), none of the investigated parameters shows an *average* that explains its surprising mechanical behaviour (Table 4). However, no other sintered alumina contains elongated crystals with similarly large (apparent) aspect ratios (Table 5). If the upper limit of the apparent distribution is an indication of the real length of anisotropically grown crystals, their 'true' aspect ratio in (C) will be about 8, but their volume content is only 5–10%. Assuming that the aspect ratio is not constant, the content of grains with an aspect ratio of more than 5 must be expected to be less than 5%. However, 5–10 vol% of SiC whiskers were required to increase the toughness of an alumina-based composite to about 4·5–6·5 MPa$\sqrt{m}$ (with contributions not only from the shape of the whiskers but additionally from interface effects and residual

Table 5. Upper limits of the frequency distributions of form anisotropy factors R and R_{orth}

Microstructure	*Average aspect ratio*	*Upper limits of frequency distributions for shape anisotropy parameters*	
	R	R^{max}	$R_{orth}{}^{max}$
Submicrometre sintered alumina (grain sizes 0·2–0·8 μm)			
(a) more uniform microstructures	1·35–1·55	3·3 ± 0·3	2·9 ± 0·2
(b) more anisotropic samples	1·75–1·85	5·0 ± 1·3	3·8 ± 0·2
Sintered alumina with grain sizes 0·9–2 μm			
(a) more uniform microstructures	1·35–1·55	3·8 ± 0·3	3·1 ± 0·3
(b) more anisotropic samples	2·00–2·40	6·2 ± 1·0	5·2 ± 0·9
Sol–gel derived microstructures from Figs 2 and 3			
Uniform sample (A), grain size 0·38 μm	1·54	3·0	2·5
Sample SG1, grain size 1·72 μm	2·40	5·0	4·9
		[24vol% > (R = 3)]	[24vol% > (R_{orth} = 2·5)]
Sample (C), grain size 1·56 μm	2·03	8·0	6·0
		[7vol% > (R = 3)]	[13vol% > (R_{orth} = 2·5)]
		[1vol% > (R = 5)]	[0·2vol% > (R_{orth} = 5)]

stresses).[21] No theoretical approach is known that predicts a significant toughness increment caused by only < 5% of particles with aspect ratios $R = 5$–10 (at $L_{max} < 4\ \mu m$) or with $R = 2$–3 at $L_{max} = 4 - 10\ \mu m$ like that observed in alumina (C). With the small size of most of the grains with large aspect ratios (Fig. 7), it becomes impossible to explain the toughness of ceramic (C) by volume content and *average* shape and size of anisotropically grown grains—in spite of the unusually large aspect ratios observed only in this microstructure. With the large body of evidence that the toughness of sintered alumina is almost independent of grain sizes in the range 0·4–4 μm,[3] it is also impossible to associate the high K_{Ic} of the material (C) with its relatively 'coarse' average grain size of 1·56 μm. On the other hand, a substantiated understanding of toughness effects cannot be derived from shape and grain size alone but needs additional investigations of grain boundary strength and crack path characteristics: even with large aspect ratios little toughening is obtained when strong interfacial bonding causes unstable bridging with only one first row of elongated particles operating in the wake.[22] It can, therefore, be speculated that weaker interfaces caused by dopants in material (C) contribute to an increased toughness, but at present neither microstructural evidence nor the available toughness models enable a reliable explanation.

6 Conclusions

The 3-dimensional equiaxed or non-equiaxed character of sintered alumina microstructures with small aspect ratios is well distinguished by Saltykov's 2-dimensional shape parameter $\overline{\Phi}_2$ on (thermally etched) cross-sections. However, $\overline{\Phi}_2$ must not be used to measure the *degree* of anisotropy of non-uniform bodies. For anisotropically grown crystals with small aspect ratios, the degree of deviations from an equiaxed character is most reliably given by $R_{orth} = L_{max}/L_{orth}$ (arbitrary sections required). In strongly anisotropic microstructures where the deviation from equiaxed shapes is large, R_{orth} or other investigated parameters do not show an advantage compared with the 'usual' aspect ratio R. The present results demonstrate that the performance of the different form anisotropy factors depends on the actual microstructure. Probably, typical differences between shape parameters as observed here will be similar when applied to other ceramics with similar microstructures (e.g. tetragonal ZrO_2).

Hard experimental evidence by all of the investigated parameters shows that none of the investigated, very different (fine-grained) alumina microstructures are equiaxed. With the term equiaxed defined long ago as a shape with exactly equal axes it is obvious that equiaxed microstructures will be extremely difficult (if not impossible) to prepare, whereas advanced technologies *approach* this aim by delivering increasingly uniform shapes.

Within the limits of fine-grained microstructures with small average aspect ratios R, significantly anisotropic shapes were observed even in microstructures with grain sizes of only 0·5 μm or less. The largest aspect ratios in all of the investigated ceramics were observed with $R = 8$ in the extremely tough material (C) for grains with an apparent maximum grain length $L_{max} = 1$–2 μm. A way to obtain anisotropic shapes in very fine-grained microstructure is indicated by processing-related differences: the anisotropic character was much more obvious in sol–gel-derived samples than in specimens prepared by powder technologies. A straightforward explanation is the larger extent of grain growth in sol–gel-derived aluminas (grain size ratio of the sintered microstructure and the

raw material is more than 10). On the other hand, fairly uniform microstructures were prepared also with larger grain sizes of 1 μm and more which means that either in sol–gel alumina grain growth is not necessarily anisotropic, and the preparation of fairly uniform microstructures is always possible.

Neither the occurrence of (relatively small) grains with larger aspect ratios $R = 5$–8 nor the existence of less than 1% of larger grains ($L_{max} > 4\mu$m) with small aspect ratios $R = 1{\cdot}5$–3 explains the surprisingly high toughness of the material (C). It is suggested that future understanding requires a 3-dimensional analysis of the remarkable bimodal correlation of shape anisotropy and grain size (Fig. 7) and an analysis of the grain boundary structure.

References

1. Krell, A. and Blank, P., Grain size dependence of hardness in dense submicrometer alumina. *J. Am. Ceram. Soc.*, 1995, **78**, 1118–1120.
2. Krell, A. and Klaffke, D., Effects of grain size and humidity on fretting wear in fine-grained alumina, Al_2O_3/TiC, and zirconia. *J. Am. Ceram. Soc.*, 1996, **79**, 1139–1146.
3. Krell, A. and Blank, P., The influence of shaping method on the grain size dependence of strength in dense submicrometre alumina. *J. Europ. Ceram. Soc.*, 1996, **16**, 1189–1200.
4. Krell, A., Blank, P., Wagner, E. and Bartels, G., Advances in the grinding efficiency of sintered alumina abrasives. *J. Am. Ceram. Soc.*, 1996, **79**, 763–769.
5. Pezzotti, G., On the actual contribution of crack deflection in toughening platelet reinforced brittle-matrix composites. *Acta Metall. et Mater.*, 1993, **41**, 1825–1839.
6. Faber, K. T. and Evans, A. G., Crack deflection processes—I. theory. *Acta Metall.*, 1983, **31**, 565–576.
7. Erikson, D. D. and Wood, W. W., *In-situ* Magnetoplumbite Growth in Sol/Gel-Derived Alumina Matrices, In *Advances in Ceramic Matrix Composites 11, Vol. 46 Ceramic Transactions*, ed. J. P. Singh and N. P. Bansal, The American Ceramic Society, Westerville OH. 1994, pp. 463–474.
8. Chantikul, P., Bennison, S. J. and Lawn, B. R., Role of grain size in the strength and R-curve properties of alumina. *J. Am. Ceram. Soc.*, 1990, **72**, 2419–2427.
9. Lutz, H. E., Hu, X. Z. and Swain, M. V., Crack tip bridging stresses in alumina and duplex ceramics. *J. Europ. Ceram. Soc.*, 1992, **9**, 133–142.
10. Koyama, T. and Niihara, N., US Patent No. US-5403795, 1995.
11. Horn, D. S. and Messing, G. L., Anisotropic Grain Growth in TiO_2-doped Alumina. *Mater. Sci. Eng A.*, 1995, **195**, 169–178.
12. Staehler, J. M., Predebon, W. W. and Pletka, B. J., A high-purity alumina with exceptional compressive and flexural strength behavior or Alumina revisited—but much better than ever. Manuscript presented at the Army Symposium on Solid Mechanics, Plymouth (MA), 4–7 November 1991.
13. Serra, J., *Image Analyses and Mathematical Morphology*, Academic Press, London, 1982, pp. 336–337.
14. Underwood, E. E., Quantitative shape parameters for microstructural features. *Microscope*, 1976, **24**, 49–64.
15. Saltykov, S. A. *Stereometrische Metallographie (Stereometrical metallography*, extended German edition of the Russian original). Deutscher Verlag für Grundstoffindustrie, Leipzig, 1974.
16. Coble, R. L., Sintering crystalline solids, I. Intermediate and final state diffusion models. *J. Appl. Physics*, 1961, **32**, 787–792.
17. Burger, W., Gernsheimer, S., Andersch, H., Friedrich, K., Lehmann, S., Schneider, J. and Fripan. M., *Sinterformkörper und seine Verwendung (Sintered Body and Application Thereof*—in German). World Patent Application WO-92/2470 Al, published February 20th 1992.
18. Gruffel, P. and Carry, C., Effect of grain size on yttrium grain boundary segregation in fine-grained alumina. *J. Europ. Ceram. Soc.*, 1993, **11**, 189–199.
19. Erikson, D. D. and Wood, W. W., US Patent No. US-5489318, 1996.
20. Cahoon, H. P. and Christensen, C. J., Sintering and grain growth of alpha-alumina. *J. Am. Ceram. Soc.*, 1956, **39**, 337–344.
21. Tiegs, T. N. and Becher, P. F., Sintered Al_2O_3-SiC-whisker composites. *Bull. Am. Ceram. Soc.*, 1987, **66**, 339–342.
22. Pezzotti, G., Okamoto, Y., Nishida, T. and Sakai, M., On the near-tip toughening by crack-face bridging in particulate and platelet-reinforced ceramics. *Acta mater.*, 1996, **44**, 899–914.